Frontiers of Physics
https://doi.org/10.1007/s11467-018-0867-y
Front. Phys.
14(1), 13608 (2019)

SUPPLEMENTAL MATERIAL

Stacking transition in rhombohedral graphite

Tataiana Latychevskaia[1,*], Seok-Kyun Son[2,3,*], Yaping Yang[2,3], Dale Chancellor[2,3], Michael Brown[2,3], Servet Ozdemir[2,3], Ivan Madan[1], Gabriele Berruto[1], Fabrizio Carbone[1], Artem Mishchenko[2,3], Kostya Novoselov[2,3,‡]

[1]*Institute of Physics, Laboratory for Ultrafast Microscopy and Electron Scattering (LUMES), École Polytechnique Fédérale de Lausanne (EPFL), CH-1015 Lausanne, Switzerland*

[2]*National Graphene Institute, University of Manchester, Oxford Road, Manchester, M13 9PL, UK*

[3]*School of Physics and Astronomy, University of Manchester, Oxford Road, Manchester, M13 9PL, UK*

Corresponding author. E-mail: [‡]*Konstantin.Novoselov@manchester.ac.uk*

1. Raman 2D-peak fitting

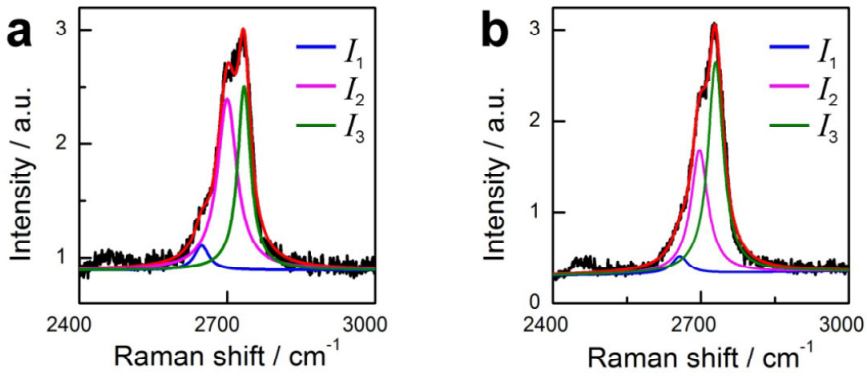

Fig. S1 Raman 2D peak fitting with 3 Lorentzian functions for ABC **(a)** and ABA **(b)**.

2. Joule heating measurement and thermal driving force calculation

The following model was considered to explain the transition from ABC to ABA stacking during the Joule heating measurement. A rectangular bar of graphite crystal with length l, width w, and thickness d, that consists of two domains, ABC and ABA domains, can be represented as two resistors in series. When a bias voltage is applied along the device, the supplied electric power is transformed into Joule heating, leading to an increase of temperature. During the Joule heating measurement, the current increases approximately linearly as a function of the applied bias voltage (the measured dependency is

*The first authors contributed equally.

shown in Fig. S2a) and thus it can be assumed that Ohm's law holds for the device and the power dissipated by Joule heating can be expressed as $P = I^2 R$ (Fig. S2b).

A temperature change caused by Joule heating results in a thermal expansion governed by the thermal expansion coefficient $\alpha(T)$. If each domain expands at a different rate, there will be a net force creating a stress at the DW which in turn can create a phase transition from ABC to ABA stacking. It is assumed that the specific heat capacity of ABC and ABA stacked domains is identical because both stacking structures have equal degrees of freedom and very similar atomic densities. The thermal expansion coefficient is also assumed to be the same for both stackings. Therefore, the difference in resistivity can produce a stress at the DW upon the applied bias voltage.

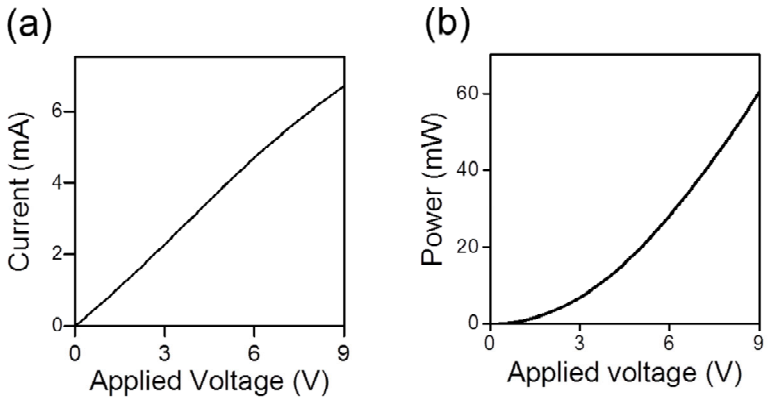

Fig. S2 Characteristics of the hBN/ABC FLG/hBN device during the Joule-heating measurements. **(a)** The measured current-voltage characteristics and **(b)** electric power-voltage characteristics calculated from (a).

To further simplify the analysis, a one-dimensional model of the temperature distribution along the device is considered. It is assumed that the ABC domain covers approximately the entire bar and the ABA domain is located near one end of the bar. The boundary conditions are such that both ends of the bar remain in thermal equilibrium with the surroundings at the ambient temperature of $T_0 = 300$ K.

By solving the one-dimensional heat diffusion equation for the case of a rectangular bar with dimensions as described above, we obtain the temperature distribution as a function of distance x counted from the centre of the bar, which is given by

$$T(x) = T_0 + \frac{p}{2g}\left[1 - \frac{\cosh(mx)}{\cosh(ml/2)}\right], \tag{S1}$$

where g is the out-of-plane thermal conductance, p is the power per unit area, $m = \sqrt{\frac{2g}{kd}}$, and k is the in-plane thermal conductivity of the bar [1]. The stress, σ_{dT} at the DW for an increase in temperature dT of the ABC domain is given by

$$\sigma_{dT} = C_{11} \cdot \alpha(T) \cdot \mathrm{d}T, \tag{S2}$$

where C_{11} is the elastic modulus along the direction of stress and strain, and $\alpha(T)$ is the in-plane thermal expansion coefficient of graphene [2]. The increase in temperature at a given point x is given by $\mathrm{d}T(x) = T(x) - T_0$, where $T(x)$ is provided by Eq. (S1).

The collected luminescence spectrum at 8 V was fitted with a grey-body radiation model modulated by a spectral line shape of the second mode of the cavity[1]. The extracted temperature was ~1200 K, from which the value of $g = 4.3 \times 10^6\,\mathrm{W \cdot m^{-2} \cdot K^{-1}}$ was calculated. A constant value of thermal expansion coefficient, $\alpha = 28 \times 10^{-6}\,\mathrm{K^{-1}}$ was used in Eq. (S2) [2], whilst the true value varies as a function of temperature [3, 4].

A DW pressure was calculated from the measured 2D-peak Raman map as follows. The voltage at which the transition occurred was evaluated from Fig. 2c, the power per unit area was calculated from Fig. S2b, the temperature decrease was obtained from Eq. (S1), and finally the critical pressure for the transition was calculated from Eq. (S2).

3. In-situ electron microscope

The employed ultrafast electron microscope (UEM) is sketched in Fig. S3. The microscope is a modified JEOL JEM-2100 TEM, based on thermionic gun technology. The electrons are emitted by a LaB_6 cathode with truncated-cone geometry. In this work, the microscope allowed studying structural changes under optical illumination (local heating) at camera-rate speed (100 ms).

The ultrafast laser pulses were generated in a regenerative Ti:Sapph amplifier with variable repetition rate (10 Hz – 1 MHz), then focused to the specimen via a lens with 250 mm focal length. The pulse duration was measured to be 60 fs, wavelength 790 nm, polarization linear, and the spatial FWHM of the beam at the specimen plane approximately 22 μm.

Single-pulse excitation (type 1 experiment) was realized combing the opening of a mechanical shutter (opening time ~120 ms) with the laser operating at 10 Hz. By monitoring a reflection of the beam on an oscilloscope, we made sure to have a single, isolated, pulse.

The trains of laser pulses (type 2 experiment) were also realized by employing the mechanical shutter and the laser system at variable repetition rates (from 10 Hz to 100 kHz).

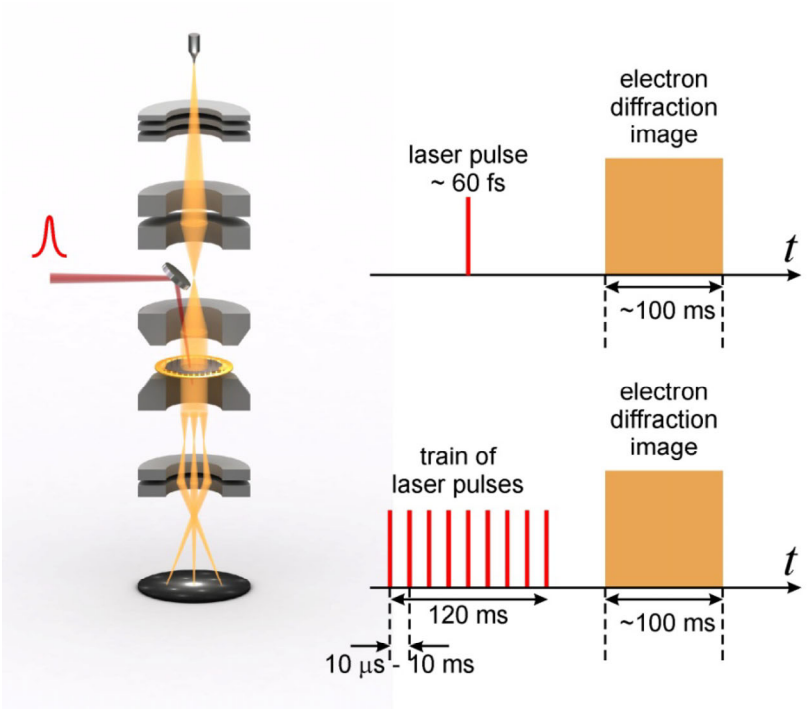

Fig. S3 Schematics of the electron microscope with optical in-situ excitation.

4. Lattice temperature evolution in FLG

The temperature evolution after single pulse optical excitation of fluences of ~150 mJ/cm^2 of a 2.5 nm thick FLG was calculated by solving the heat diffusion equation for a suspended region of FLG. The obtained distribution is shown in Fig. S4.

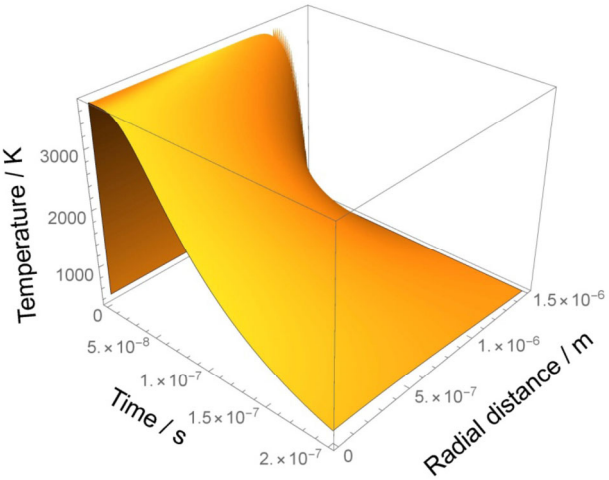

Fig. S4 Lattice temperature evolution in graphene after optical excitation.

5. Electron diffraction patterns simulations

Diffraction patterns of graphene structures were simulated as follows. The far-field distribution of the scattered wavefront was calculated as a sum of waves scattered off individual atoms [5]:

$$\Psi_l\left(K_x,K_y\right)=\sum_i L\left(\vec{r}_i\right)\exp\left[-i\left(K_x x_i+K_y y_i\right)\right]\exp\left(-iz_i\sqrt{K^2-K_x^2-K_y^2}\right),$$

where *K*-coordinates are introduced as $\vec{K}=\left(K_x,K_y,K_z\right)=k\frac{\vec{R}}{R}=\frac{2\pi}{\lambda R}\left(X,Y,Z\right),\ \left|\vec{K}\right|=k=\frac{2\pi}{\lambda},$ $K_z=\sqrt{K^2-K_x^2-K_y^2}$, $\vec{R}=\left(X,Y,Z\right)$ is the coordinate in the detector plane, i runs through all the atoms in the lattice, $\vec{r}_i$ are the coordinates of the atoms (exact coordinates, not in pixels), and l is the layer number, $l=1...L$, L - total number of layers. The diffraction patterns were then calculated as

$$I\left(K_x,K_y\right)=\frac{1}{L}\left|f\left(K_x,K_y\right)\right|^2\left|\sum_{l=1}^{L}\Psi_l\left(K_x,K_y\right)\right|^2,$$

where $\left|f\left(K_x,K_y\right)\right|^2=\left|f\left(\vartheta\right)\right|^2=\frac{\mathrm{d}\sigma}{\mathrm{d}\Omega}$ is the scattering cross-section which accounts for scattering amplitude $f\left(\vartheta\right)$ dependency on the scattering angle ϑ. The values of the scattering cross-section $\frac{\mathrm{d}\sigma}{\mathrm{d}\Omega}$ for carbon at 200 keV electron energy were obtained from the NIST Electron Elastic-Scattering Cross-Section Database [6]. Radial intensity profiles of simulated diffraction patterns for *L* = 3,6,7,8 and 9 are shown in Fig. S4. From the intensity profiles it is evident that the intensity distribution does not significantly depend on the number of layers. However, there is a small difference. The peak at *k* = 4.7 nm^{-1} which is observed for ABA stacking (Fig. S4a) is absent for ABC stacking when the number of layers is an integer of 3 (*L* = 3,6,...) and it is very weak when the number of layers is not an integer of 3 (*L* = 7,8...), Fig. S4b, c.

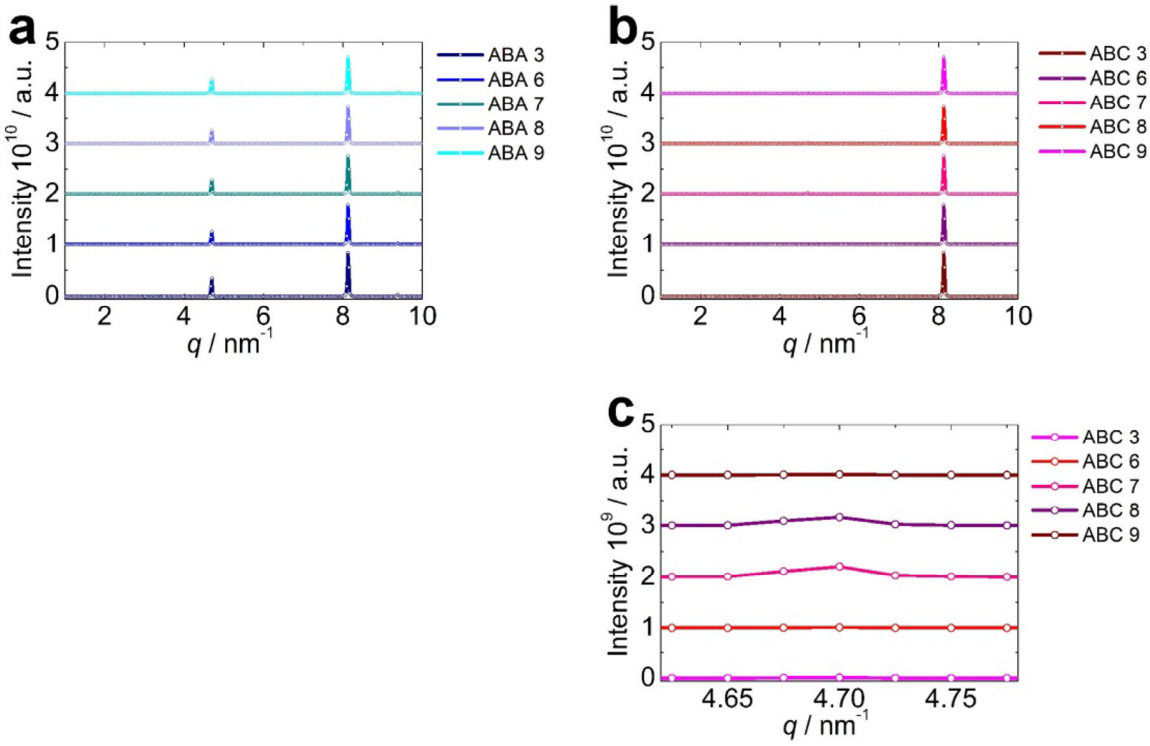

Fig. S5 Radial intensity profiles of simulated diffraction patterns for 3,6,7,8 and 9 graphene layers arranged in **(a)** ABA stacking, and **(b, c)** ABC stacking. Here, $q = k \sin \vartheta$, where $k = 2\pi / \lambda$, λ is the wavelength and ϑ is the scattering angle.

References

1. S. K. Son, C. Mullan, J. Yin, V. G. Kravets, A. Kozikov, S. Ozdemir, M. Alhazmi, M. Holwill, K. Watanabe, T. Taniguchi, D. Ghazaryan, K. S. Novoselov, V. I. Fal'ko, and A. Mishchenko, Graphene hot-electron light bulb: incandescence from hBN-encapsulated graphene in air, *2D Materials* **5**, 011006 (2018)

2. I. Shabalin, Ultra-High Temperature Materials, Springer, 2016

3. B. T. Kelly, The high temperature thermal expansion of graphite parallel to the hexagonal axis, *Carbon* **10**, 435 (1972)

4. W. C. Morgan, Thermal expansion coefficients of graphite crystals, *Carbon* **10**, 73 (1972)

5. T. Latychevskaia, C. R. Woods, Y. B. Wang, M. Holwill, E. Prestat, S. J. Haigh, and K. S. Novoselov, Convergent beam electron holography for analysis of van der Waals heterostructures, *Proceedings of the National Academy of Sciences* **115**, 7473 (2018)

6. A. Jablonski, NIST Electron Elastic-Scattering Cross-Section Database, NIST Standard Reference Database 64 (2010)